Ocean response to meridional ekman transport in the Atlantic and implication for gravity missions

Alexandre Ganachaud[1] and Herlé Mercier

Laboratoire de Physique des Océans, CNRS IFREMER UBO, Plouzané France

Received 9 April 2002; accepted 18 July 2002; published 14 December 2002.

[1] Wind friction at the ocean surface introduces energetic variations in the net mass transport across the oceanic basins. To conserve mass, the whole water column adjusts rapidly, introducing a depth-independent perturbation in the pressure field. This signal is analyzed in a high resolution numerical model of the Atlantic Ocean. While the pressure perturbation cannot be extracted from the energetic sea surface height signals, it represents up to 90% of the bottom pressure signal when integrated across the Atlantic Ocean in the daily and monthly frequencies. This signal will be an important part of the signal measured by the GRACE (Gravity Recovery And Climate Experiment) mission. *INDEX TERMS:* 1223 Geodesy and Gravity: Ocean/Earth/atmosphere interactions (3339); 1227 Geodesy and Gravity: Planetary geodesy and gravity (5420, 5714, 6019); 4556 Oceanography: Physical: Sea level variations. **Citation:** Ganachaud, A., and H. Mercier, Ocean response to meridional ekman transport in the Atlantic and implication for gravity missions, *Geophys. Res. Lett.*, *29*(23), 2145, doi:10.1029/2002GL015291, 2002.

1. Introduction

[2] With the recent launch of GRACE to measure the earth's gravity field and its variations, it has become important to identify the oceanic signals that are measurable and relevant. *Wahr et al.* [1998] used an ocean general circulation model to estimate that the satellite-to-satellite tracking GRACE mission would recover bottom pressure signals of 1 mbar magnitude with an accuracy of 0.1 mbar over spatial scales of 500 km. Similarly, *Ponte* [1999] calculated the seasonal variability in bottom pressure at 1 to several mbar, depending upon the region.

[3] Variations in the ocean surface winds induce large changes in the oceanic Ekman transport due to friction at the ocean surface. The wind fluctuations are energetic over a broad frequency range. Although confined to the surface, Ekman transport affects the whole water column and the associated property transports such as the meridional heat transports [*Jayne and Morotzke*, 2001]. Because mass is conserved almost instantaneously in the Atlantic Ocean north of a zonal line, the water column has to adjust within a few hours. According to linear theory, this adjustment is depth-independent and geostrophic over a large spatio-temporal range [*Willebrand et al.*, 1980], resulting in a vertically uniform pressure perturbation.

[4] There is no appropriate data to test the Ekman transport response process that we describe, and a numerical ocean model had to be used. The high resolution CLIPPER model appeared appropriate as it reproduces the circulation and its variability relatively faithfully [*Tréguier et al.*, 2001]. CLIPPER is a primitive equation model at 1/6° resolution for the Atlantic Ocean with open boundaries at the South. There is a rigid lid with 42 geopotential levels narrowly spaced near the surface. Open boundaries are defined, in Drake Passage and South of Africa; buffer zones are defined next to the closed boundaries in the Cadix Gulf and at 70°N, where the net transports is fixed at 1 Sv southward. After an initialization to seasonal climatology followed by an 8-year spin-up, daily forcing is applied based on ECMWF reanalysis (1979–1993) and analysis (1994–1999). At the surface, the mixed layer is represented through a second order closure model. The output fields consist of five-day averages of temperature, salinity, surface pressure gradients and wind stress forcing from 1995 to 1997. Most of the variability related with the large scale wind field is captured, the latter having a red spectrum for periods of one month and shorter [*Salby*, 1992, p.102].

2. Ocean Response to Ekman Transport

[5] The meridional Ekman transport may be calculated as

$$T_{Ek}(x,t) = -\tau^x(x,t)/f, \qquad (1)$$

where x is the longitudinal distance; t is time; τ^x is the zonal wind stress and f is the Coriolis parameter. While there is not much observational evidence to validate this simple calculation at large scales, it has not been proven wrong [e.g., *Chereskin and Roemmich*, 1991]. Figure 1 shows the average and variability (one standard deviation) of the net meridional Ekman transport from 5-day averages over the Atlantic Ocean. The transport is determined not only by wind, but also by latitude (through f) and basin width. The variability is close to 4 Sv rms (1 Sv = 10^6 m^3 s^{-1}) everywhere except near the Equator where (1) is no longer valid (f = 0). This variability exceeds the time-mean Ekman transport except in the Trade winds and in the Southern Westerlies. Correlation between local wind stress and its zonal integral suggests that the variability in the meridional transport is driven by wind changes over large regions centered on the basin rather than by localized regions of high wind variability. The Ekman transport spectrum is red at high frequencies, with in the North Atlantic 82% of energy being in the 3 year-20 day range and 18% in 20–10 day.

2.1. Ocean Response

[6] Variations in meridional Ekman transport are followed by the generation of gravity waves to insure quasi instantaneous mass conservation across the basin. In the present numerical model, gravity waves have infinite veloc-

[1]Now at Institut de Recherche pour le Développement, New Caledonia.

0094-8276/02/2002GL015291$05.00

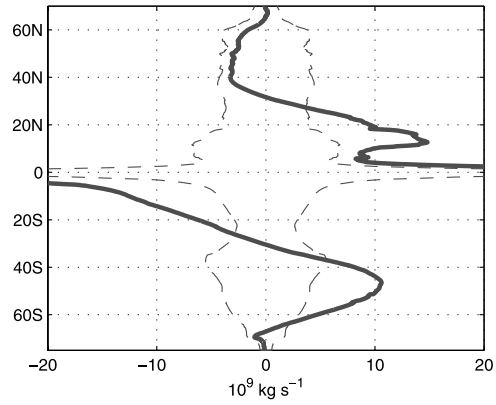

Figure 1. Meridional Ekman transport over the Atlantic. The thick line indicates the time-average over 4 years (1995–1999) while the dashed line indicates the variability (± one standard deviation). Transports, positive northward, are calculated from the ECMWF wind products using (1).

ities due to the rigid lid approximation so that mass conservation is absolute (in the model the conservation is of volume, not exactly mass). Numerical models with a free surface such as the one of *Jayne and Marotzke* [2001], do not depart from conservation by more than ±1 Sv (see their Figure 1). Altimetric data show no evidence for large scale mass storage other than the 2 mm/yr secular trend [*Cabanes et al.*, 2001]. In addition, the ocean response is believed to be geostrophic for periods above the inertial period ($2\pi f^{-1}$ $\simeq$ 24 hours at 30°N).

[7] Figure 2 shows this balance at 26°N, between the Ekman transport and the net meridional geostrophic flow in the model. The latter is calculated from the absolute pressure field (hydrostatics + surface pressure gradient). There is a small ageostrophic imbalance that is dominated by the time derivative in the momentum balance equation. Coherence, or correlation within frequency bands, between the net meridional Ekman transport *Tek* and (a) the local Ekman transport *Tek*(x) (b) the meridional geostrophic velocity over the whole water column sheds light on the dynamical characteristics of the response.

[8] In the monthly range (20–81 day), coherence with meridional velocities is spread over the basin rather than regionally confined (Figure 3, upper). Phase structures of 500 km wavelengths are apparent. Coherence and phase lines are vertical almost everywhere below 1000 m, indicating that the response to changes in *Tek* is depth-independent. Such a response is expected for an atmospheric forcing that occurs on scales larger than 1000 km and at periods between a few 100 days and the inertial period [e.g., *Willebrand et al.*, 1980]. The adjustment occurs through westward propagating barotropic Rossby waves, as indicated by Hovmüller diagrams (not shown). In the upper 1000 m, the coherence is lower due to variability from sources other than Ekman that dominates the signals.

[9] For longer time scales (90 day-3 year band; not shown), the coherence still shows waves with more structure in the vertical, indicating more baroclinic motions as expected at low frequencies. The wavelengths range 300–500 km. In contrast, at high frequencies (10–20 day band, not shown) the coherence with net Ekman transport is significant just east of the mid-Atlantic Ridge and over a thin band in the middle of the eastern basin. East of the mid-Atlantic Ridge, the coherence corresponds to the maximum coherence with local Ekman transport *Tek*(x), suggesting local forcing, as expected at high frequencies [*Willebrand et al.*, 1980].

[10] Similar properties are noticed at 48°, 32° and 9°N, with more baroclinic signals in the yearly band for the latter. At mid-latitudes the response to meridional Ekman transport changes is therefore depth-independent for periods in the range 10–90 days. Westward propagating planetary waves are generated, except at high frequencies where the response is local. A projection on linear oceanic wave modes [*Wunsch*, 1997] shows that 50% of the kinetic energy (all frequencies) lies in the first baroclinic mode and 20% in the first barotropic mode. (In such projection, the barotropic mode is defined as the depth-average velocity so that the upper ocean variability dominates both the baroclinic and barotropic modes, with the two modes cancelling out in the deep ocean.) Because near-surface variability is high, the signal in sea surface height that corresponds to the response to Ekman transport changes is buried in other signals, and no coherence is found at any time scales. This contradicts results from non-eddy-resolving models suggesting that sea surface height signals are of barotropic nature at periods shorter than one month [*Stammer et al.*, 2000]. While the relative importance of the Ekman-related signal is found to be greater at depth, the total energy is lower.

2.2. Bottom Pressure Response

[11] Geostrophic balance between Ekman transports and return flow may be written approximately as [*Ponte and Rosen*, 1994]

$$\int_W^E dx\, h(x) \frac{1}{f} \frac{\partial p_b'}{\partial x}(x,t) \simeq -\int_W^E dx\, T_{Ek}'(x,t), \qquad (2)$$

where prime variables are perturbations from time-averages; $h(x)$ is depth; ρ is density and p_b is the bottom pressure and the prime denotes a perturbation from time mean. For constant depth, the left hand side (2) reduces to the east-

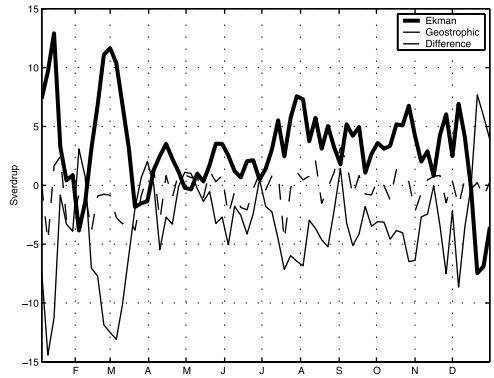

Figure 2. Ekman and geostrophic balance. The thick line shows the meridional Ekman transport calculated from the wind stress at 26.8°N while the thin line shows the geostrophic flow that quasi balances the Ekman transport (all quantities are 5-day averages). The dashed line shows the residual departure from geostrophic balance.

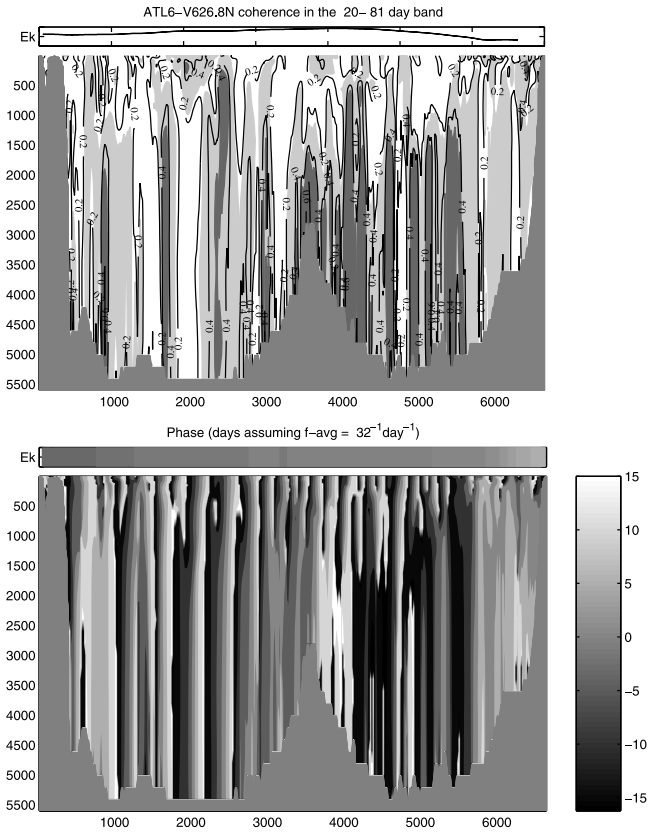

Figure 3. Coherence and phase at 26.8°N. The upper graphic shows the coherence between net meridional Ekman transport ($\int dx T_{Ek}(x)$) and meridional geostrophic velocities $v(x, z)$ in the 20–81 day frequency range. X-axis is zonal distance (km); Y-axis is depth (m). The clear shaded area shows locations where coherence is non-zero at more than 60% confidence level; the dark shaded area at 95%. The coherence and phase (days) between net and local ($T_{Ek}(x)$) Ekman transport is indicated in the upper bars above the graphics with scale from zero to one; 95% confidence for non-zero coherence is 0.45.

west cross-basin bottom pressure difference. Note that (2) does not require assumption of depth-independance.

[12] Figures 4 to 6 show the squared coherence between both sides of (2) for the daily, monthly and yearly frequency band as previously defined and at each latitude. The coherence is high and significant nearly everywhere in the daily band (Figure 4) except in the Equatorial band (±10°), where ocean dynamics differ from (2). In the South Atlantic, the phase lag is close to 1 day, the theoretical time for Ekman and geostrophic transports to establish. (The lag is interpreted as the sum of the delay between the wind shift and the establishment of the Ekman currents at the surface plus the delay to achieve geostrophic balance in the return flow.)

[13] In the monthly band (Figure 5) the coherence is also high and significant away from the Equator. The magnitude is similar to that of the daily band; the phase indicates a lag between 0 and 5 days, depending on latitude. In the North Atlantic, the lag is close to zero, while in the South Atlantic it lies between 2 and 5 days. At periods of 3 months and longer (Figure 6), the coherence varies abruptly with

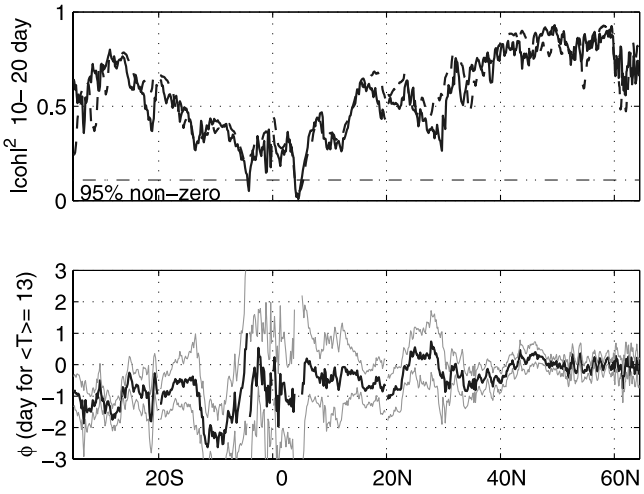

Figure 4. (Thick line) Squared coherence and phase between net Ekman transport and geostrophic flow from bottom pressure gradient as a function of latitude in the frequency band 10^{-1}–20^{-1}day $^{-1}$. The phase is expressed in units of days for the average frequency over the band which is 13^{-1}day^{-1}; phase is given only for locations where coherence is significant at the 95% confidence level. The confidence interval on phase is of $1.96 \times \sqrt{(c^{-2} - 1/2m)}$ where c is coherence and m is the number of frequencies over which it is calculated. The dashed line in the upper plot indicates the coherence from spatially filtered fields (see text).

latitude; it is significant on 70% of the latitudes. The phase is generally indistinguishable from zero due to the lower coherence (not shown). However, a significant phase lead of up to one month is visible at 13°S and 63°N, possibly indicating a resonance such as the excitation of basin modes in the monthly frequency band [*LaCasce and Pedlosky*, 2002].

[14] The generally high coherence indicates that the geostrophic response to Ekman transport is an important signal in the bottom pressure gradients. In an analysis of the ocean angular momentum, *Ponte and Rosen* [1994] found

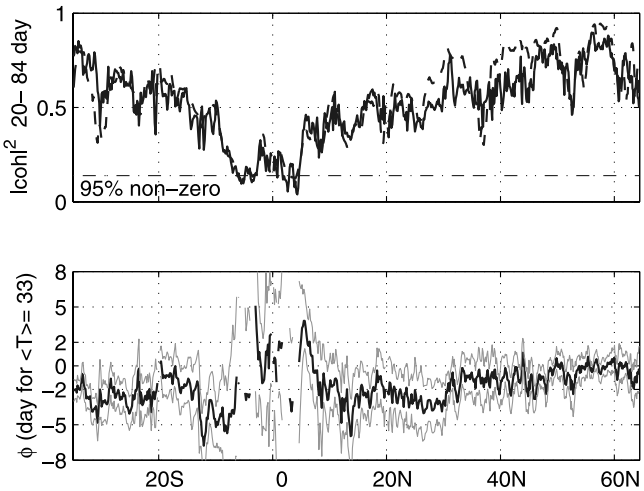

Figure 5. Same as Figure 4, but for the yearly frequency band, 20^{-1} –84^{-1}day^{-1}.

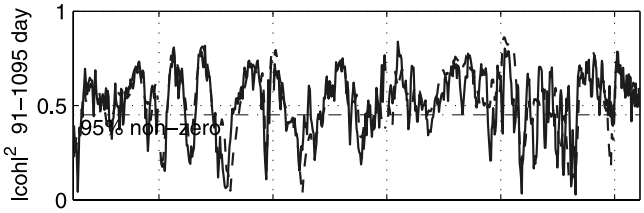

Figure 6. Same as Figure 4, but for the yearly frequency band, 91^{-1} day^{-1}–3^{-1}yr^{-1}.

that bottom pressure torques were in balance with surface wind torques-a similar conclusion.

3. Implication for Space Gravity Missions

[15] The gravity perturbations detected by satellites includes, in addition to the ocean mass (i.e., the bottom pressure), several other signals such as the continental ground water and variations in atmospheric mass [*Wahr et al.*, 1998]. For GRACE, all signals will be measured over scales of about 300 km, for an accuracy of about 0.4 cm in equivalent water thickness [*Wahr et al.*, 1998, Figure 6]. For a constant-depth ocean of 4000 m, a perturbation of 0.4 cm corresponds to a mass transport of 1.6 Sv at mid-latitudes-a signal/noise ration of 6.2 in the Atlantic. To simulate the satellite measurements, the bottom pressure gradients were spatially filtered with a Loess [*Schlax and Chelton*, 1992] filter with cutoff at 300 km. Coherence between the Ekman transport (meridionally filtered at 300 km for consistency) and the geostrophic transport calculated from the filtered bottom pressure gradients is similar to the non-filtered one (Figures 4–6, upper dashed lines), as is the phase (not shown). Our results are therefore not affected by the limited spatial resolution of the satellite and the gravimetric data should contain up to 90% of the Ekman signal at all frequencies permitted by the sampling. We chose to work with bottom pressure gradients for consistency with the model grid (equivalently, one could average the bottom pressure perturbations as done by satellites).

[16] Another issue of the gravity recovery is the aliasing of frequencies that are higher than the temporal resolution-30 days for the GRACE mission. The exact effect of aliasing can be simulated as for altimetry using the orbital sampling [*Tierney et al.*, 2000; *Stammer et al.*, 2000]-with a more complete model including all geopotential sources. About 5% (20% in the tropics) of the energy of the meridional Ekman-related signals lie in the 20–10 day frequency range, and therefore is subject to being aliased in the GRACE signal.

4. Discussion and Conclusion

[17] Variations in meridional Ekman transports are important at all frequencies down to about 10 days. In the realistic numerical model that we used, the ocean reaction is fast and almost independent of depth, yielding a measurable signature in the pressure perturbations. However, this signature is not measurable by altimeters, the signal being overwhelmed by upper ocean variability in the same frequency range-in contradiction with previous works based on lower resolution models. The signature is in principle measurable by gravity missions such as GRACE and we show that the signal is 80% to 90% of the zonally integrated bottom pressure signals. Nevertheless, other types of signals may limit detectability if not properly modelled. We chose to focus on a specific aspect of the gravity signals while gravity missions will provide new insights on many other aspects of ocean circulation [*Committee on Earth Gravity from Space*, 1997]. In particular, the spatial resolution will allow to better monitor strong currents and recirculations that are not apparent in the meridional transports. In addition to a better understanding of the content of the gravity signal, our method may provide a test for evaluating wind products and Ekman theory on large scales.

[18] **Acknowledgments.** We thank two anonymous reviewers, P. LeGrand, G. Reverdin, A.-M. Treguier, P. Klein, and R. Ponte for their helpful comments and S. Michel and F. Lyard for their assistance. Supported by CNES and PNTS. The code for the Loess filter was provided by the LEGOS (Toulouse).

References

Cabanes, C., C. Le Provost, and A. Cazenave, Sea level rise during past 40 years from satellite and in situ observations, *Science*, *294*, 840–842, 2001.

Chereskin, T. K., and D. Roemmich, A comparison of measured and wind-driven Ekman transport at 11°N in the Atlantic Ocean, *J. Phys. Oceanogr.*, *21*, 869–878, 1991.

Committee on Earth Gravity from Space, Satellite gravity and the geosphere, Tech. rep., National Academy of Sciences, National Academy Press, Washington, D.C., 1997.

Jayne, S. R., and J. Marotzke, The dynamics of ocean heat transport variability, *Rev. of Geophys.*, *39*, 385–411, 2001.

LaCasce, J., and J. Pedlosky, Baroclinic Rossby waves in irregular basins, *J. Phys. Oceanogr.*, submitted, 2002.

Ponte, R., A preliminary model study of the large-scale seasonal cycle in bottom pressure over the global ocean, *JGR*, *104*, 1289–1300, 1999.

Ponte, R., and R. Rosen, Oceanic angular momentum and torques in a general circulation model, *J. Phys. Oceanogr.*, *24*, 1966–1977, 1994.

Salby, M., The atmospherein *Climate system modeling* edited by K. Trenberth, pp. 53–116, Cambridge University Press, Cambridge, UK, 1992.

Schlax, M., and D. Chelton, Frequency domain diagnostics for linear smoothers, *J. Amer. Statistical Assoc.*, *87*, 1070–1081, 1992.

Stammer, D., C. Wunsch, and R. Ponte, De-aliasing of global high frequency barotropic motions in altimeter observations, *Geophys. Res. Lett.*, *27*, 1175–1178, 2000.

Tierney, C., J. Wahr, F. Bryan, and V. Zlotnicki, Short-period oceanic circulation: Implication for satellite altimetry, *Geophys. Res. Lett.*, *27*, 1255–1258, 2000.

Tréguier, A. M., et al., An eddy permitting model of the Atlantic Circulation: Evaluating open boundary conditions, *J. Geophys. Res.*, *106*, 22,115–22,129, 2001.

Wahr, J., M. Molenaar, and F. Bryan, Time variability of the Earth's gravity field: Hydrological and oceanic effects and their possible detection using GRACE, *J. Geophys. Res.*, *103*, 30,205–30,229, 1998.

Willebrand, J., S. G. H. Philander, and R. C. Pacanowski, The oceanic response to large-scale atmospheric disturbances, *J. Phys. Oceanogr.*, *10*, 411–429, 1980.

Wunsch, C., The vertical partition of oceanic horizontal kinetic energy, *J. Phys. Oceanogr.*, *27*, 1770–1794, 1997.

A. Ganachaud and H. Mercier, Laboratoire de Physique des Océans, CNRS IFREMER UBO, Plouzané, France.